Real-time Estimation of States and Unknown Boundary Conditions in Pressurized Pipeline Systems

Morteza Imani[1], Aaron Zecchin[2], Wei Zeng[3], Martin F. Lambert[4]

[1]PhD Candidate; School of Architecture and Civil Engineering, University of Adelaide, SA 5005, Australia; Email: morteza.imani@adelaide.edu.au

[2]Senior Lecturer; School of Architecture and Civil Engineering, University of Adelaide, SA 5005, Australia; Email: aaron.zecchin@adelaide.edu.au

[3]Lecturer; School of Architecture and Civil Engineering, University of Adelaide, SA 5005, Australia; Email: w.zeng@adelaide.edu.au

[4]Professor; School of Architecture and Civil Engineering, University of Adelaide, SA 5005, Australia; Email: martin.lambert@adelaide.edu.au

Abstract

Accurate estimation of boundary conditions in pressurized pipelines is essential for effective monitoring, control, and fault detection. However, boundary variables such as unmeasured demands and unknown pressure heads are often unavailable, introducing uncertainty into hydraulic models. This study presents a real-time observer-based framework for joint estimation of system states and unknown boundary inputs. The approach employs the Elastic Water Column Model (EWCM) to derive a linear time-invariant (LTI) representation compatible with observer design. Because the system does not satisfy the observer matching condition, auxiliary outputs are generated to transform it into a matched form. These outputs are first estimated using a High-Gain Observer (HGO) and then incorporated into a Sliding Mode Observer (SMO) for reconstructing both states and boundary conditions.

The framework is validated through two numerical case studies and laboratory experiments involving transient pipeline flows. Results demonstrate accurate real-time estimation of unknown boundary conditions using only internal pressure data. Compared with batch-based methods such as Expectation–Maximization and Weighted Least Squares, the proposed observer-based strategy provides a computationally efficient and real-time alternative for hydraulic system monitoring.

Keywords: Dynamic state estimation, Unknown boundary conditions, Elastic water column model, High-gain observer, Sliding mode observer.

Introduction

The accurate estimation of system states and unknown inputs is a fundamental challenge in many engineering applications, including fluid mechanics, control systems, and structural health monitoring [1-3]. In pressurized pipeline systems, this challenge is particularly prominent due to the inherent limitations in sensor coverage and the dynamic interactions between boundary conditions and internal states. Inflows and outflows are often unmonitored or only partially observed, and pressure sensors may be deployed sparsely due to cost or accessibility constraints. These factors introduce uncertainty into hydraulic models, reducing their effectiveness for monitoring, fault detection, and real-time control [4, 5]. In practical settings, boundary conditions such as pressure variations at reservoirs, connections of sub-networks to broader systems or unmeasured consumer demands are not always directly observable. For example, while a pipeline may be equipped with internal pressure sensors, the influence of changes at the boundaries may not be reflected in the measured outputs in a straightforward manner. Moreover, pipeline systems are subject to external disturbances and

varying operational regimes, which make it difficult to maintain accurate state awareness using traditional modeling techniques.

Traditional approaches to handling these uncertainties often rely on optimization-based techniques such as Expectation-Maximization (EM), Weighted Least Squares (WLS), and Inverse Transient Analysis (ITA) [6-10]. These methods typically operate in batch mode, requiring historical data and iterative parameter tuning. While suitable for offline analysis, their high computational demands and dependency on prior data limit their application in real-time monitoring or control environments. Moreover, these approaches often assume that uncertainties are fixed over time or follow specific statistical models, which may not hold under dynamically changing operating conditions.

These limitations motivate the development of an approach capable of real-time estimation using observer-based methods rather than iterative optimization. A promising alternative arises from state observers, which reconstruct unmeasured states and inputs dynamically from limited measurements. A class of such observers, known as UIOs, has been developed to estimate internal states while decoupling the effect of unknown inputs [11-14]. UIOs are designed such that the estimation error is insensitive to unmeasured disturbances, allowing for reliable state reconstruction. Depending on the application, UIOs can be implemented in centralized or distributed forms. In centralized implementations, all measurements are processed together to estimate the complete system state. In contrast, distributed observers achieve estimation cooperatively across interconnected subsystems, each using local information and limited data exchange [15]. Such designs are particularly relevant for large-scale systems, as demonstrated in the distributed interval observer and distributed UIO formulations presented in[16]. These studies show how observer-based estimation can be extended to networked or multi-agent systems.

Other developments have aimed to improve convergence speed or robustness. For instance, prescribed-time UIOs for descriptor systems [17] and their distributed counterparts [18] guarantee convergence within a user-specified time window using structure decomposition and prescribed-time convergence tools. These contributions broaden applicability to descriptor (singular) and multi-agent systems where strict timing is critical. However, such prescribed-time designs are primarily relevant to aerospace or robotic systems, whereas hydraulic systems evolve on slower time scales, and convergence within a fixed time window is generally unnecessary.

Despite their versatility, classical UIOs require two strict mathematical conditions: the observer matching condition (OMC) and the minimum-phase condition [19, 20]. The OMC ensures that the unknown input affects the system through the same channel as the measured outputs. In hydraulic terms, this means that if an unknown input (e.g., a leak or unmeasured demand) appears in the continuity equation for a given node, a pressure measurement must also be available at that same location. This co-location guarantees that the influence of the unknown input is reflected in the output, allowing the observer to infer it. When this condition is satisfied, a UIO can be designed directly. However, in most practical hydraulic systems, sensors are not co-located with uncertain boundaries, producing unmatched conditions that violate the OMC and make direct observer design infeasible.

This mismatch renders the estimation problem mathematically underdetermined, with fewer independent equations than unknowns. To overcome this, researchers have developed various strategies to relax or bypass the OMC and minimum-phase requirements. A key line of work, pioneered by Kalsi et al. and Floquet et al., introduced the use of differentiated auxiliary outputs and a two-stage structure combining HGOs and SMOs [21-23]. The approach differentiates measured signals until the unknown inputs appear explicitly in the output equations, thereby transforming the system into a form that satisfies the matching condition. Because these

differentiated outputs are not directly measurable, they must first be estimated by an HGO, after which an SMO reconstructs both the system states and unknown inputs. This two-stage strategy effectively extends UIO applicability to systems that do not naturally meet the OMC, and similar two-observer frameworks have also been employed for sensor fault estimation and fault-tolerant control in nonlinear systems, such as the 3-DOF helicopter study by Wang and Tan [24], where a combined HGO–SMO structure enabled accurate fault reconstruction despite unmatched and non-minimum-phase dynamics.

Subsequent studies have also addressed the minimum-phase condition, developing formulations that enable observer design even in non-minimum-phase or nonlinear settings [25]. Parallel advances have expanded UIO-related concepts to enhance robustness against modeling uncertainties and disturbances. For example, interval-based observer designs [16, 26, 27] have been proposed to provide guaranteed bounds on state estimates and improve robustness to model uncertainty. In a different direction, the left-invertibility formulation by Zhang and Zhu [28] introduced a constructive method to augment measured outputs so that the OMC can be satisfied even when auxiliary-output approaches fail. Their method is particularly useful when no relative-degree-based augmentation can recover the required rank condition. These theoretical developments have established a strong mathematical foundation for extending observer-based estimation to broader classes of systems.

Despite this progress, most of the above works have been developed in aerospace, robotic, and electrical domains, where the physical processes and measurement architectures differ fundamentally from those of hydraulic systems. To date, no systematic framework has been established for applying UIO or SMO concepts to pressurized pipelines, even though such systems naturally exhibit unmatched boundary conditions, sparse sensor deployment, and uncertain disturbances.

The present study addresses this gap by introducing a real-time observer-based framework for hydraulic pipelines. A linear state-space model is first derived using the EWCM, which reformulates the transient flow equations into a structure suitable for observer design. Auxiliary outputs are generated using a HGO, and a SMO is applied to jointly estimate internal states and unknown boundary conditions. The use of HGOs enables estimation of unmeasured variables without requiring explicit statistical noise models, while SMOs provide robustness against bounded disturbances and modeling errors.

The novelty of this work lies in bridging the gap between established observer theory and its application to hydraulic pipelines. Specifically, the contributions are: (i) the development of a linear state-space formulation of pipelines using the EWCM that is suitable for observer design; (ii) the integration of HGOs and SMOs in a two-stage structure to overcome the OMC and enable real-time estimation; and (iii) the first experimental demonstration of observer-based reconstruction of unknown boundary conditions in pressurized pipelines. To evaluate the performance of the proposed framework, two numerical case studies have been conducted. The first case involves the estimation of an unmeasured demand based on internal pressure data, reflecting a common situation in hydraulic monitoring where unknow withdrawals occur at certain locations. The second case concerns the estimation of unknown boundary pressures using only internal sensor data, a scenario highly relevant to real-time control. In addition to simulations, experimental validation has been performed on a laboratory pipeline setup where two boundary heads has been estimated by the purposed approach. The remainder of this paper is structured as follows. Section 2 introduces the EWCM and its discretization, leading to a state-space formulation. Section 3 describes the observer design, detailing the use of HGOs for auxiliary output estimation and SMOs for joint state and unknown input estimation. Section 4 presents the results from two numerical simulations and Section 5 presents the experimental validation. Finally, Section 6 concludes the paper and outlines directions for future research,

including potential extensions to larger pipeline networks with multiple unmeasured boundary conditions.

Elastic Water Column Model

The behavior of transient flow in pressurized pipeline systems is governed by the one-dimensional partial differential equations of momentum and continuity. These equations describe the relationship between pressure head, flow rate, and system dynamics, incorporating the effects of fluid compressibility and pipe elasticity. The governing equations are expressed as [29]:

$$\frac{\partial h}{\partial x}+\frac{1}{g\mathcal{A}}\frac{\partial q}{\partial t}+\frac{fq|q|}{2gD\mathcal{A}^2}=0 \tag{1}$$

$$\frac{g\mathcal{A}}{a^2}\frac{\partial h}{\partial t}+\frac{\partial q}{\partial x}=0 \tag{2}$$

where h represents the piezometric head, q is the volumetric flow rate, g is the gravitational acceleration, $\mathcal{A}$ is the internal cross-sectional area of the pipe, D is the pipe diameter, and f is the Darcy-Weisbach friction factor. These equations provide a continuous representation of transient flow, capturing wave propagation effects due to the compressibility of water and elasticity of pipes. For practical applications, a pipeline section of length l is often analyzed under the assumption of spatially uniform conditions, approximating the spatial derivatives as finite differences ($\partial h/\partial x \approx \Delta h/l$ and $\partial q/\partial x \approx \Delta q/l$). This results in a discrete form of the transient flow equations [30]:

$$\Delta h=-L\frac{\partial q}{\partial t}-Rq|q| \tag{3}$$

$$\Delta q=-C\frac{\partial h}{\partial t} \tag{4}$$

where L is the hydraulic inductance $\left(L = \frac{l}{g\mathcal{A}}\right)$, C is the hydraulic capacitance $\left(C = \frac{gAl}{a^2}\right)$, and R is the hydraulic resistance $\left(R = \frac{fl}{2gD\mathcal{A}^2}\right)$. The electrical equivalent circuit is often used to approximate hydraulic behavior, where the pipe segment is modeled using a π-type circuit representation [31, 32]. Fig. 1 shows the electrical equivalent circuit for two segments of a pipe.

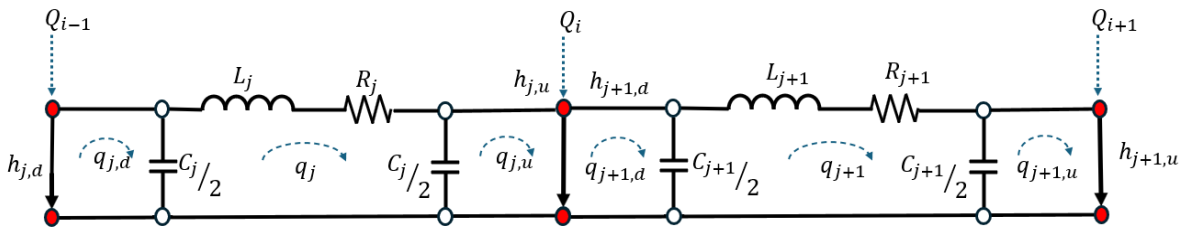

Fig. 1. Electrical Equivalent Circuits for two segments of a pipe.

To capture higher frequencies, the pipeline can be divided into segments. The first two nodes are designated as head boundary nodes, while the remaining nodes serve as internal nodes. External demands can be considered at the locations of internal nodes. For a structured mathematical formulation, the nodal head vector is partitioned as:

$$\boldsymbol{h} = \begin{bmatrix} \boldsymbol{h}_I \\ \boldsymbol{h}_R \end{bmatrix} \tag{5}$$

where $\boldsymbol{h}_I$ represents the heads at internal nodes, and $\boldsymbol{h}_R$ corresponds to the heads at boundary nodes. Using this partitioning, the vector of head differences across each pipeline segment is expressed as:

$$\Delta\boldsymbol{h} = \begin{bmatrix} \mathbf{M}_I \\ \mathbf{M}_R \end{bmatrix}^{\intercal} \begin{bmatrix} \boldsymbol{h}_I \\ \boldsymbol{h}_R \end{bmatrix} \tag{6}$$

Where $^{\intercal}$ operator represents the transpose operator, and the matrices $\mathbf{M}_I$ and $\mathbf{M}_B$ are defined as:

$$\mathbf{M}_I \in \mathbb{R}^{(n_s-1)\times n_s},\ \boldsymbol{M}_{I_{i,j}} = \begin{cases} -1 & if\ j = i \\ 1 & if\ j = i+1 \\ 0 & otherwise \end{cases} \quad \boldsymbol{M}_{R_{i,j}} = \begin{bmatrix} 1 & 0_{(1\times(n_s-1))} \\ 0_{(1\times(n_s-1))} & -1 \end{bmatrix} \tag{7}$$

Following the formulation in [31], the demand vector $\boldsymbol{Q}$ and the hydraulic parameter matrices $\boldsymbol{L}$, $\boldsymbol{R}$, and $\boldsymbol{C}$ (all diagonal) are incorporated into the momentum and continuity equations governing the pipeline system. The momentum equation is given by:

$$\boldsymbol{L}\frac{d\boldsymbol{q}}{dt} = -\boldsymbol{R}\mathrm{diag}\{|\boldsymbol{q}|\}\boldsymbol{q} + \mathbf{M}_I^{\mathrm{T}}\boldsymbol{h}_I + \mathbf{M}_R^{\mathrm{T}}\boldsymbol{h}_R \tag{8}$$

where $|\boldsymbol{q}|$ represents the element-wise absolute value of the flow rate vector (hereon, the absolute value function of a vector or matrix represents an elementwise operation). The continuity. The continuity equation at internal nodes is expressed as:

$$\left(\frac{1}{2}|\mathbf{M}_I|\boldsymbol{C}\right)\frac{d\boldsymbol{h}_I}{dt} = \mathbf{M}_I\boldsymbol{q} + \boldsymbol{Q} \tag{9}$$

Eq. (14) and (15) constitute a system of nonlinear ODEs for transient simulation of a pipeline. This formulation has been validated using the Method of Characteristics, and further details can be found in [31].

Nonlinear System Representation

Eq. (8) and Eq. (9) can be expressed in a compact state-space form. To achieve this, the state vector $\boldsymbol{x}$ is defined to include both the flow rates through the pipes and the hydraulic heads at the internal nodes:

$$\boldsymbol{x} = \begin{bmatrix} \boldsymbol{q} \\ \boldsymbol{h}_I \end{bmatrix} \tag{10}$$

The inputs to the system are the hydraulic heads at the boundary nodes and the external demands applied at internal locations:

$$\boldsymbol{u} = \begin{bmatrix} \boldsymbol{h}_R \\ \boldsymbol{Q} \end{bmatrix} \tag{11}$$

In this formulation, the system's nonlinear dynamics can be expressed as:

$$\dot{\boldsymbol{x}} = f(\boldsymbol{x}, \boldsymbol{u}) \tag{12}$$

This equation describes how the state vector $\boldsymbol{x}$ evolves over time as a nonlinear function $f(\boldsymbol{x}, \boldsymbol{u})$ of the state and the inputs. Solving this equation provides the complete transient response of the pipeline to changes in external demands or boundary conditions, capturing both flow rates and hydraulic heads along the system.

Linearization and State-Space Representation

To apply observer-based estimation techniques, the nonlinear EWCM model needs to be expressed in a LTI form. Since EWCM is inherently nonlinear, linearization is performed around a steady-state operating point to obtain a state-space representation suitable for real-time estimation. This is achieved by expanding the system dynamics $f(\boldsymbol{x}, \boldsymbol{u})$ in a first-order Taylor series around the equilibrium point $\boldsymbol{x}_0, \boldsymbol{u}_0$ leading to the linearized state-space representation [33]:

$$\dot{\boldsymbol{x}} = \boldsymbol{A}\boldsymbol{x} + \boldsymbol{B}\boldsymbol{u} \tag{13}$$

Here, $\boldsymbol{A}$ and $\boldsymbol{B}$ are the Jacobian matrices of partial derivatives with respect to the state and input, respectively. The system matrix $\boldsymbol{A}$ characterizes how flow rates and hydraulic heads evolve in response to perturbations in the state, while the input matrix $\boldsymbol{B}$ describes how external inputs, such as boundary conditions or demand variations, influence the system. The structure of $\boldsymbol{A}$ depends on the spatial discretization of the pipeline and its hydraulic properties. In practical applications, the dynamics in Eq. (13) are also affected by modeling uncertainty, sensor noise, and unmeasured boundary disturbances. These effects are collectively represented by an additional input term $\boldsymbol{D}\boldsymbol{w}$, where $\boldsymbol{w}$ denotes unknown or unmeasured inputs such as fluctuating reservoir heads or demand variations. The linearized model can therefore be expressed as $\dot{\boldsymbol{x}} = \boldsymbol{A}\boldsymbol{x} + \boldsymbol{B}\boldsymbol{u} + \boldsymbol{D}\boldsymbol{w}$, which serves as the basis for unknown-input observer design.

Observer based state estimation

In many real-world dynamic systems, including single pipelines, certain inputs remain unknown or unmeasurable due to sensor limitations, external disturbances, or uncertain boundary conditions. Estimating both the internal states and these unknown inputs is crucial for effective monitoring and control. UIO provide a mathematical framework to estimate system states while accounting for such unknown inputs. In this context, the UIO is not itself the physical quantity being estimated, but rather the estimation mechanism used to reconstruct both the internal states $\boldsymbol{x}$ and the unknown boundary conditions, which appear mathematically as components of the disturbance vector $\boldsymbol{w}$.

Classical UIO and the Observer Matching Condition

A LTI system with unknown inputs can be generally expressed as[34]:

$$\begin{aligned} \dot{\boldsymbol{x}} &= \boldsymbol{A}\boldsymbol{x} + \boldsymbol{B}\boldsymbol{u} + \boldsymbol{D}\boldsymbol{w} \\ \boldsymbol{y} &= \boldsymbol{C}\boldsymbol{x} \end{aligned} \tag{14}$$

where the state vector $\boldsymbol{x}$ consists of the system's flow rates and hydraulic heads. The number of pipes in the network is denoted by n_p, while the number of internal nodes is represented by n_i. As a result, $\boldsymbol{x}$ is a column vector of dimension $(n_p + n_i) \times 1$, capturing the complete hydraulic state of the pipeline system. The measured output vector y represents the available sensor readings, such as pressure measurements at specific locations within the network. The number of sensors deployed determines the dimension of $\boldsymbol{y}$, which is p.

The known input vector $\boldsymbol{u}$ includes control inputs, such as boundary conditions at monitored locations, reservoir heads, or external demands applied at specific nodes. The dimension of known inputs is m_1. The unknown input vector $\boldsymbol{w}$ accounts for disturbances and unmeasured

boundary conditions, and the number of unknown inputs is m_2. $\boldsymbol{A}$, $\boldsymbol{B}$, $\boldsymbol{C}$, $\boldsymbol{D}$ are known fixed matrices of appropriate dimension.

An UIO is designed to estimate $\boldsymbol{x}$ independently of $\boldsymbol{w}$, ensuring that the state estimation error is not affected by the unknown inputs. However, a fundamental requirement for designing a classical UIO is the observer matching condition, which states that the unknown input $\boldsymbol{w}$ must appear in the same subspace as the measured output $\boldsymbol{y}$. Mathematically, this condition is:

$$\text{rank}\{\boldsymbol{CD}\} = \text{rank}\{\boldsymbol{D}\} = m_2$$

which ensures that the unknown input does not introduce an unobservable mode in the system. When this condition is not satisfied, the unknown input is said to be unmatched, meaning it does not directly appear in the measured output channel. As a result, a classical UIO cannot be used in such cases. In hydraulic systems, unknown boundary conditions (such as unmeasured heads, leaks, or demand variations) often do not directly affect the measured outputs in a way that satisfies the observer matching condition and $\text{rank}\{\boldsymbol{CD}\} < m_2$. This creates a fundamental challenge in real-time state estimation.

To address this limitation, an auxiliary output approach is introduced, which transforms the system into a form where the unknown inputs can be reconstructed. A common strategy to circumvent the observer matching condition is to augment the output space by generating auxiliary outputs that explicitly incorporate the influence of the unknown inputs. This is achieved by differentiating the output until the unknown input explicitly appears, effectively increasing the system's observability. If the system does not satisfy the classical matching condition, the relative degree r_i of each output $\boldsymbol{y}_i$ with respect to the unknown input $\boldsymbol{w}$ is defined as the smallest integer such that [22]:

$$\begin{aligned} &\boldsymbol{C}_j\boldsymbol{A}^k\boldsymbol{D} = 0 \ \text{ for all } k < r_j - 1 \\ &\boldsymbol{C}_j\boldsymbol{A}^{r_j-1}\boldsymbol{D} \neq 0 \end{aligned} \tag{15}$$

This means that the unknown input $\boldsymbol{w}$ only appears in the $r_j - th$ derivative of the output $\boldsymbol{y}_j$. If all system outputs have a relative degree of one, the classical UIO can be directly applied. However, in cases where some outputs have a higher relative degree, additional differentiation is required to reveal the unknown inputs. To construct an observer that accounts for unmatched unknown inputs, an augmented output vector is introduced:

$$\boldsymbol{y}_a = \boldsymbol{C}_a\boldsymbol{x} \qquad \boldsymbol{C}_a = \begin{bmatrix} \boldsymbol{C}_1 \\ \vdots \\ \boldsymbol{C}_1\boldsymbol{A}^{\gamma_1-1} \\ \vdots \\ \boldsymbol{C}_p \\ \vdots \\ \boldsymbol{C}_p\boldsymbol{A}^{\gamma_p-1} \end{bmatrix} \tag{16}$$

where the integers $1 \leq \gamma_i \leq r_i$ are such that $r\text{ank}\{\boldsymbol{C}_a\boldsymbol{D}\} = \text{rank}\{\boldsymbol{D}\}$, while minimizing the total sum of γ_i across all outputs. Along with the matching condition, another requirement is that the system should be minimum phase, and the invariant zeros of the triple $\{\boldsymbol{A}, \boldsymbol{C}, \boldsymbol{D}\}$ must lie in the left half-plane. Floquet and Bartot also proved that the triples $\{\boldsymbol{A}, \boldsymbol{C}, \boldsymbol{D}\}$ and $\{\boldsymbol{A}, \boldsymbol{C_a}, \boldsymbol{D}\}$ have the same invariant zeros, and if the main system is minimum phase, the system with the augmented output will also be minimum phase [21].

High-Gain Observers for Auxiliary Output Estimation

Before designing the SMO for estimating system states and unknown inputs, the auxiliary outputs must first be estimated and provided as inputs to the SMO. To achieve this, let $y_{ij} = \boldsymbol{c}_i\boldsymbol{A}^{j-1}\boldsymbol{x}$ for $i = 1, \dots, p$ and $j = 1, \dots, \gamma_i$ leading to the auxiliary output vector representation: $\boldsymbol{y}_a = \begin{bmatrix} \boldsymbol{y}_{a1}^{\mathrm{T}} & \cdots & \boldsymbol{y}_{ap}^{\mathrm{T}} \end{bmatrix}^{\mathrm{T}}$, where $\boldsymbol{y}_{ai} = \boldsymbol{C}_{ai}x = [\boldsymbol{y}_{ai,1} \quad \cdots \quad \boldsymbol{y}_{ai,\gamma_i}]^{\mathrm{T}}$.

By differentiating $\boldsymbol{y}_{ai}$ with respect to time, the following expression is obtained:

$$\dot{\boldsymbol{y}}_{ai} = \boldsymbol{C}_{ai}\dot{\boldsymbol{x}} = \boldsymbol{C}_{ai}\boldsymbol{A}\boldsymbol{x} + \boldsymbol{B}\boldsymbol{u} + \boldsymbol{C}_{ai}\boldsymbol{D}\boldsymbol{w} \tag{17}$$

Introducing the following matrices:

$$\boldsymbol{\Lambda}_i = \begin{bmatrix} 0 & I_{\gamma_i-1} \\ 0 & 0 \end{bmatrix} \epsilon\, R^{\gamma_i \times \gamma_i},\ \ \boldsymbol{E}_i = \begin{bmatrix} 0_{(\gamma_i-1)\times 1} \\ 1 \end{bmatrix} \epsilon\, R^{\gamma_i}\ ,\ \boldsymbol{H}_i = \boldsymbol{C}_{ai}\boldsymbol{B} = \begin{bmatrix} \boldsymbol{c}_i\boldsymbol{B} \\ \vdots \\ \boldsymbol{c}_i\boldsymbol{A}^{\gamma_i-2}\boldsymbol{B} \\ \boldsymbol{c}_i\boldsymbol{A}^{\gamma_i-1}\boldsymbol{B} \end{bmatrix} \tag{18}$$

272 Eq. (17) can then be rewritten as:

$$\dot{\boldsymbol{y}}_{ai} = \boldsymbol{\Lambda}_i\boldsymbol{y}_{ai} + \boldsymbol{E}_i f_i(\boldsymbol{x},\boldsymbol{w}) + \boldsymbol{H}_i\boldsymbol{u} \tag{19}$$

273 where $f_i(\boldsymbol{x},\boldsymbol{w}) = \boldsymbol{c}_i\boldsymbol{A}^{\gamma_i-1}(\boldsymbol{A}\boldsymbol{x} + \boldsymbol{D}\boldsymbol{w})$. By considering $\boldsymbol{y}_{i1} = \boldsymbol{y}_i$ as the output equation, the

274 state space representation for $\boldsymbol{y}_{ai}$ is given by:

$$\begin{cases} \dot{\boldsymbol{y}}_{ai} = \boldsymbol{\Lambda}_i\boldsymbol{y}_{ai} + \boldsymbol{E}_i f_i(\boldsymbol{x},\boldsymbol{w}) + \boldsymbol{H}_i\boldsymbol{u} \\ \boldsymbol{y}_{i1} = \bar{\boldsymbol{c}}_i\boldsymbol{y}_{ai} \end{cases} \tag{20}$$

275 where $\bar{\boldsymbol{c}}_i = [1 \quad 0 \quad \ldots \quad 0]\, \epsilon\, R^{\gamma_i}$. With this formulation, the system is now suitable for the

276 design of a HGO. The following observer is constructed to estimate $\boldsymbol{y}_{ai}$:

$$\dot{\boldsymbol{y}}_{hi} = \boldsymbol{\Lambda}_i\boldsymbol{y}_{hi} + \boldsymbol{H}_i\boldsymbol{u} + \boldsymbol{l}_i\bar{\boldsymbol{c}}_i(\boldsymbol{y}_{ai} - \boldsymbol{y}_{hi}) \tag{21}$$

277 where $\boldsymbol{y}_{hi} = [\hat{\boldsymbol{y}}_{ai,1} \quad \ldots \quad \hat{\boldsymbol{y}}_{ai,\gamma_i}]^{\mathrm{T}}$. The gain vector $\boldsymbol{l}_i$ is defined as $\boldsymbol{l}_i = \left[\frac{\alpha_{ai,1}}{\varepsilon} \quad \ldots \quad \frac{\alpha_{ai,\gamma_i}}{\varepsilon^{\gamma_i}}\right]^{\mathrm{T}}$,

278 where $\varepsilon\, \epsilon\, (0,1)$ is a design parameter and $\alpha_{ai,j}, j = 1, \ldots, \gamma_i$, are selected such that the

279 characteristic polynomial $S^{\gamma_i} + \alpha_{ai,1}S^{\gamma_i-1} + \cdots + \alpha_{ai,\gamma_i-1}S + \alpha_{ai,\gamma_i} = 0$, has all roots in the

280 left half-plane, ensuring system stability [23, 35]. For the convergence analysis, the difference

281 between the actual and estimated auxiliary outputs is defined as:

$$\boldsymbol{e}_y = \boldsymbol{y}_{ai} - \boldsymbol{y}_{hi} \tag{22}$$

282 In order to simplify the analysis, the error is scaled according to:

$$\zeta_{ij} = \frac{y_{ij} - \hat{y}_{ij}}{\varepsilon^{\gamma_i - j}} \qquad j = 1, \ldots, \gamma_i, \tag{23}$$

283 The scaled error dynamics take the form:

$$\varepsilon\dot{\boldsymbol{\zeta}}_i = \bar{\boldsymbol{A}}_{ci}\boldsymbol{\zeta}_i + \varepsilon\boldsymbol{E}_i f_i(\boldsymbol{x},\boldsymbol{w}) \quad \textit{with}\ \bar{\boldsymbol{A}}_{ci} = \begin{bmatrix} -a_{ai}^{\mathrm{T}} & \boldsymbol{I}_{\gamma_i-1} \\ -a_{ai,\gamma_i} & 0_{\gamma_i-1} \end{bmatrix} \tag{24}$$

Where $a_{ai} = [a_{ai,1} \quad \cdots \quad a_{ai,(\gamma_i-1)}]$ is Hurwitz and $f_i(\boldsymbol{x}, \boldsymbol{w})$ is bounded. Since $\overline{\boldsymbol{A}}_{ci}$ is Hurwitz, the dynamics are exponentially stable, while the perturbation term is of order ε. By the result in [36], there exist positive constants $\beta_i > 0$ and finite time $T_i(\varepsilon)$ such that:

$$\|\zeta_i(t)\| \leq \beta_i \varepsilon, \quad t \geq t_0 + T_i(\varepsilon), \quad lim_{\varepsilon \to 0} T_i(\varepsilon) \tag{25}$$

From Eq. (23) it follows that

$$\boldsymbol{y}_{ai} - \boldsymbol{y}_{hi} = \boldsymbol{D}_i \boldsymbol{\zeta}_i \tag{26}$$

Where $\boldsymbol{D}_i = \text{diag}[\varepsilon^{\gamma_i - 1}, \varepsilon^{\gamma_i - 2}, \ldots, 1]$. Let

$$\boldsymbol{y}_h = \left[\boldsymbol{y}_{h1}^{\intercal}, \ldots, \boldsymbol{y}_{hp}^{\intercal}\right]^{\intercal}, \quad \boldsymbol{D} = \text{diag}\left[\boldsymbol{D}_1, \ldots, \boldsymbol{D}_p\right], \quad \boldsymbol{\zeta} = \left[\boldsymbol{\zeta}_1^{\intercal}, \ldots, \boldsymbol{\zeta}_p^{\intercal}\right]^{\intercal} \tag{27}$$

Thus, $\boldsymbol{y}_a - \boldsymbol{y}_h = \boldsymbol{D}\boldsymbol{\zeta}$. Since the Euclidean norm of **D** is unity, i.e. $\|\boldsymbol{D}\| = 1$, it follows that:

$$\|\boldsymbol{y}_a - \boldsymbol{y}_h\| \leq \beta \varepsilon \tag{28}$$

With $\beta = \left(\sum_{i=1}^{p} \beta_i^2\right)^{1/2}$. Therefore, after a short transient, the auxiliary outputs generated by the high-gain observer converge to the true derivatives with an error proportional to ε.

Sliding-mode observer construction

Once the auxiliary outputs are estimated, a SMO can be designed to estimate the system states and unknown inputs. The sliding mode observer follows the form [34]:

$$\dot{\hat{\boldsymbol{x}}} = \boldsymbol{A}\hat{\boldsymbol{x}} + \boldsymbol{B}\boldsymbol{u} + \boldsymbol{G}_l(\boldsymbol{y}_a - \boldsymbol{C}_a\hat{\boldsymbol{x}}) + \boldsymbol{G}_n \boldsymbol{v}_c \tag{29}$$

where $\boldsymbol{G}_l$ and $\boldsymbol{G}_n$ serve as observer gains, while $\boldsymbol{v}_c$ is an injection signal that is designed based on the output estimation error:

$$\boldsymbol{v}_c = \begin{cases} -\rho \dfrac{\boldsymbol{P}_2(\boldsymbol{y}_a - \boldsymbol{C}_a\hat{x})}{\|\boldsymbol{P}_2(\boldsymbol{y}_a - \boldsymbol{C}_a\hat{x})\|} & \text{if } (\boldsymbol{y}_a - \boldsymbol{C}_a\hat{\boldsymbol{x}}) \neq 0 \\ 0 \quad \text{otherwise} \end{cases} \tag{30}$$

The parameter ρ is a positive constant chosen to exceed the upper bound $\boldsymbol{w}$. The symmetric positive definite matrix $\boldsymbol{P}_2$ is defined in [20] and further detailed in Chapter 6 of [19]. This

signal ensures that the system reaches a sliding motion within the state estimation error space in finite time. The primary goal is to guarantee that the state estimation error, defined as $\boldsymbol{e} = \boldsymbol{x} - \hat{\boldsymbol{x}}$, remains asymptotically stable and unaffected by the unknown input $\boldsymbol{w}$ once the sliding motion (sliding manifold $\boldsymbol{s} = \boldsymbol{C}_a\boldsymbol{e} = 0$) is established. The estimation error dynamics can be expressed as:

$$\dot{\boldsymbol{e}} = \boldsymbol{A}\boldsymbol{e} + \boldsymbol{D}\boldsymbol{w} - \boldsymbol{G}_l(\boldsymbol{y}_a - \boldsymbol{C}_a\hat{\boldsymbol{x}}) - \boldsymbol{G}_n\boldsymbol{v}_c \tag{31}$$

During the sliding motion, the following condition holds:

$$\dot{\boldsymbol{s}} = \boldsymbol{C}_a\dot{\boldsymbol{e}} = \boldsymbol{C}_a(\boldsymbol{A} - \boldsymbol{G}_l\boldsymbol{C}_a)\boldsymbol{e} + \boldsymbol{C}_a\boldsymbol{D}\boldsymbol{w} - \boldsymbol{C}_a\boldsymbol{G}_n\boldsymbol{v}_c = 0 \tag{32}$$

Since the estimation error tends to zero $(e \to 0)$, the equivalent output rejection term satisfies $\boldsymbol{C}_a\boldsymbol{G}_n(\boldsymbol{v}_c)_{eq} \to \boldsymbol{C}_a\boldsymbol{D}\boldsymbol{w}$. This implies that once sliding motion is established, the equivalent output rejection term becomes equal to the effect of the unknown input. Given that $\boldsymbol{C}_a\boldsymbol{D}$ is a full-rank matrix, an approximation $\hat{\boldsymbol{w}}$ of the unknown input $\boldsymbol{w}$ can be obtained as[22]:

$$\hat{\boldsymbol{w}} = ((\boldsymbol{C}_a\boldsymbol{D})^{\intercal}\boldsymbol{C}_a\boldsymbol{D})^{-1}(\boldsymbol{C}_a\boldsymbol{D})^{\intercal}\boldsymbol{C}_a\boldsymbol{G}_n(\boldsymbol{v}_c)_{eq} \tag{33}$$

Numerical simulation

In this section, to demonstrate the capability of the approach, two test cases have been considered. In the first test case, an unknown demand is estimated in real time based on information from a single sensor located at another node along the pipeline. The second test case is more realistic; in this scenario, two sensors are placed along the pipeline, and the head at both ends of the pipe is estimated in real time. Such situations can naturally occur in a network, and by focusing on an isolated pipe, this approach can be effectively applied.

Test case 1: Estimating unknown demand

This test case demonstrates unknown boundary and state estimation for a single pipeline. The pipeline configuration is shown in Fig. 2.

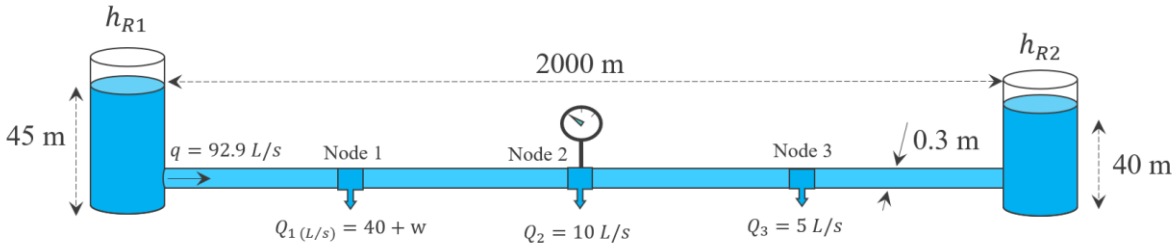

Fig. 2. Pipeline configuration for Test Case 1. The wave speed is 1000 m/s and friction factor is 0.02.

The pipeline consists of three nodes with equal spacing, and the demand at each node is specified in the figure. A pressure sensor is installed at node 2, while an uncertainty is introduced in the demand extracted at node 1. The system is initially in steady state, and at the first step, it is linearized to obtain a state-space model for observer design. The state space model for this test has been obtained as below:

$$\frac{d}{dt}\begin{bmatrix} q_1 \\ q_2 \\ q_3 \\ q_4 \\ h_1 \\ h_2 \\ h_3 \end{bmatrix} = \begin{bmatrix} -0.0876 & 0 & 0 & 0 & -0.0014 & 0 & 0 \\ 0 & -0.0499 & 0 & 0 & 0.0014 & -0.0014 & 0 \\ 0 & 0 & -0.0405 & 0 & 0 & 0.0014 & -0.0014 \\ 0 & 0 & 0 & -0.0357 & 0 & 0 & 0.0014 \\ 2884.2 & -2884.2 & 0 & 0 & 0 & 0 & 0 \\ 0 & 2884.2 & -2884.2 & 0 & 0 & 0 & 0 \\ 0 & 0 & 2884.2 & -2884.2 & 0 & 0 & 0 \end{bmatrix} \times \begin{bmatrix} q_1 \\ q_2 \\ q_3 \\ q_4 \\ h_1 \\ h_2 \\ h_3 \end{bmatrix} +$$

$$\begin{bmatrix} 0 & 0 & 0 & 0.0014 & 0 \\ 0 & 0 & 0 & 0 & 0 \\ 0 & 0 & 0 & 0 & 0 \\ 0 & 0 & 0 & 0 & -0.0014 \\ -2884.2 & 0 & 0 & 0 & 0 \\ 0 & -2884.2 & 0 & 0 & 0 \\ 0 & 0 & -2884.2 & 0 & 0 \end{bmatrix} \times \begin{bmatrix} Q_1 \\ Q_2 \\ Q_3 \\ h_{R1} \\ h_{R2} \end{bmatrix} + \begin{bmatrix} 0 \\ 0 \\ 0 \\ 0 \\ -2884.2 \\ 0 \\ 0 \end{bmatrix} w \tag{34}$$

$$y = [0 \quad 0 \quad 0 \quad 0 \quad 0 \quad 1 \quad 0] \times \begin{bmatrix} q_1 \\ q_2 \\ q_3 \\ q_4 \\ h_1 \\ h_2 \\ h_3 \end{bmatrix}$$

By using the "*tzero*" function in MATLAB, it can be easily verified that the system is minimum phase and can be applied to the proposed method. This property is physically justified by the fact that hydraulic pipeline systems are dissipative due to friction and contain no external energy sources, making them inherently passive and stable. As a result, the states that are not

directly influenced by inputs or outputs do not lead to instability. Based on the state-space representation, the uncertainty acts in the same input channel as the known demand (Q_1). The rank of the $\boldsymbol{CD}$ matrix is zero, while the rank of the $\boldsymbol{D}$ matrix is one, indicating that the necessary condition for directly applying a SMO is not satisfied. To address this, an auxiliary output is introduced to meet the observability condition.

Using Eq. (15), the relative degree of the output is determined as 2, meaning:

$$\begin{aligned} &\boldsymbol{CD} = 0 \\ &\boldsymbol{CAD} = 0 \\ &\boldsymbol{CA^2D} \neq 0 \end{aligned} \tag{35}$$

This result indicates that two auxiliary outputs are required. A HGO is designed to estimate these outputs, with design parameters chosen as $\varepsilon = 0.001$ and $\alpha_{a,1,..4} = [1, 9, 26, 24]$. The coefficients of the characteristic polynomial ($\alpha_{a,1,..4}$) have been chosen such that all roots lie in the left half-plane. The SMO is then designed following the approach detailed in [37], and the observer gain matrices are computed accordingly:

$$\boldsymbol{G_n} = \begin{bmatrix} 0 & 0 & 0 \\ -3.12e3 & -15.63 & 1.13^{-13} \\ -3.12^{-3} & -19.63 & 1.7^{-13} \\ 0 & 0 & 0 \\ 918.4 & 5.1861 & -2884.2 \\ 1.15^{4} & 0 & 0 \\ 918.4 & 5.1861 & 0 \end{bmatrix} \quad \boldsymbol{G_l} = \begin{bmatrix} 1.1^{-4} & -6.2^{-7} & -3.4^{-4} \\ -27.59 & -0.139 & -3.4^{-4} \\ -27.59 & -0.175 & 0 \\ 1.1^{-4} & 6.23^{-7} & 0 \\ 788.8 & 3.954 & 26 \\ 102 & 01 & 0 \\ -772.5 & -4.86 & 0 \end{bmatrix} \tag{36}$$

For the SMO design, the uncertainty must be bounded, and the ρ parameter should be set larger than the upper bound of the uncertainty. In this test case, $\rho = 100$ is chosen, ensuring fast rejection of uncertainties. There is no strict limitation on the selection of ρ, as long as it is sufficiently large. Fig. 3 presents the MATLAB Simulink implementation of the proposed approach.

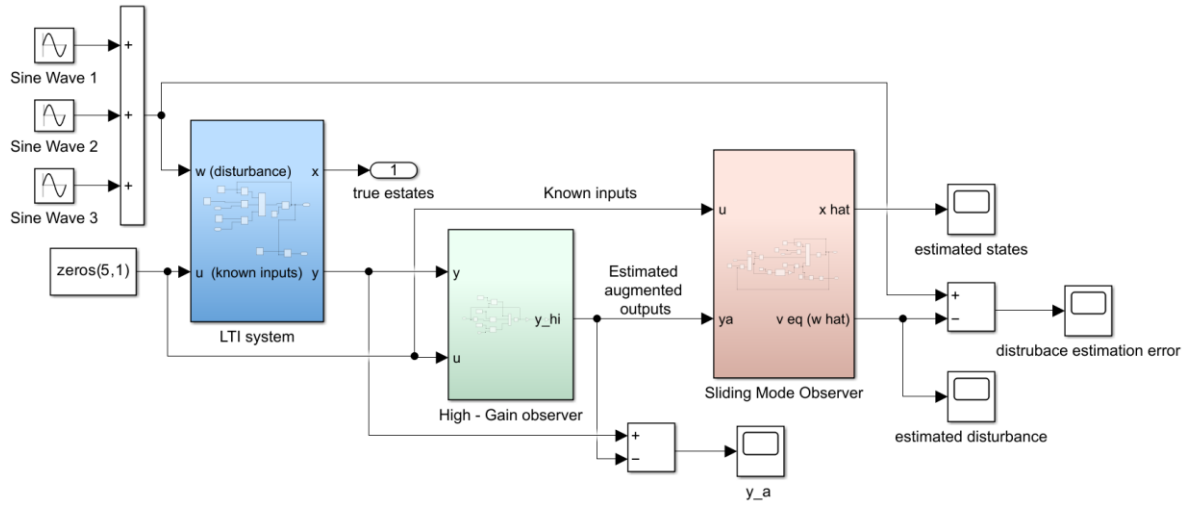

Fig. 3. Simulink model for Test Case 1.

The true disturbance acting on the system is generated as a summation of three sine waves with amplitudes of 10, 5, and 2 L/s and frequencies of 0.1, 0.15, and 0.18 Hz, respectively. The disturbance can be any arbitrary signal. Fig. 4a compares the true and estimated disturbances, showing a close match between the estimated and actual values. Fig. 4b presents the absolute estimation errors, which remain small. Additionally, the observer demonstrates fast convergence, reaching the actual disturbance within less than one second.

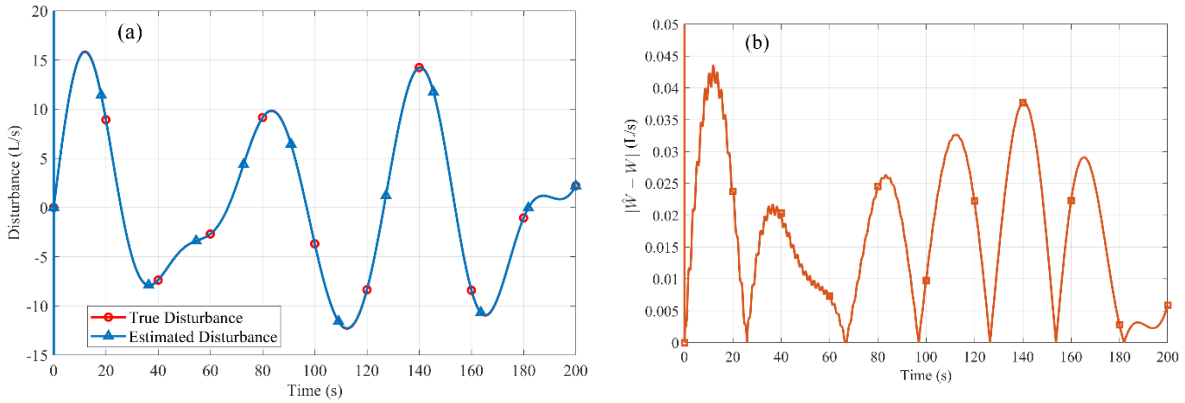

Fig. 4. Disturbance estimation results: (a) comparison between the true and estimated disturbances, and (b) the absolute estimation error over time

Fig. 5 illustrates the error between the estimated auxiliary outputs (computed by HGO) and their actual values. It is observed that y_{a2}, the first auxiliary output (i.e., the first derivative of the measured output), is estimated more accurately than y_{a3}, which represents the second

derivative. Nevertheless, the overall estimation errors for both remain small. As the order of auxiliary outputs increases, estimation accuracy slightly decreases but remains within an acceptable range.

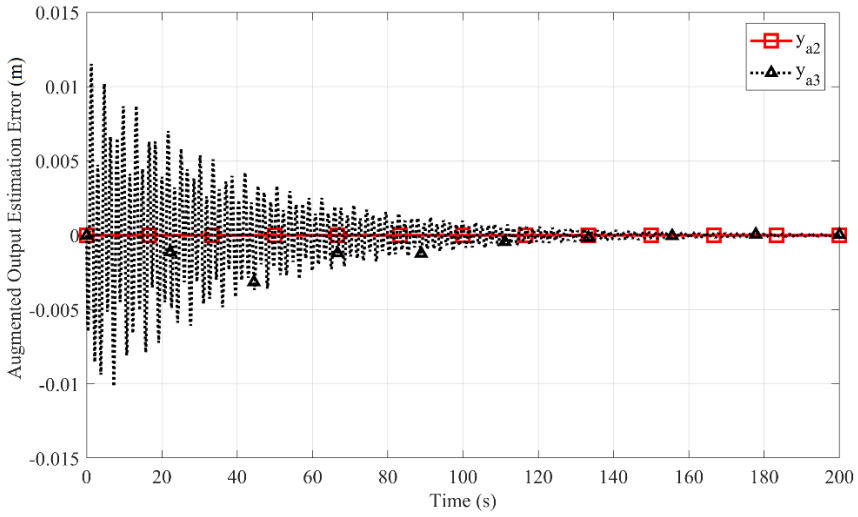

Fig. 5. Auxiliary output estimation error.

The SMO observer is also capable of estimating the system states, as shown in Fig. 6. In this figure, the internal pressure head from both the estimation and the true simulation is shown, demonstrating a close match between the two. Since the system is linearized, these values represent the head change relative to the fixed point. During the first 80 seconds after applying the disturbance, the system experiences a transient response before transitioning to a steady oscillatory state.

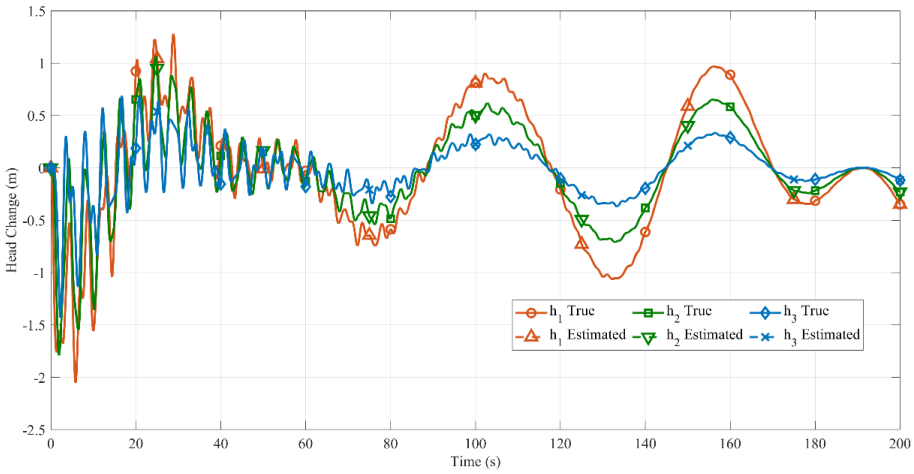

Fig. 6. Comparison of true and estimated internal pressure head state variables for Test Case 1.

Test Case 2: Estimating unknown heads

The pipeline configuration and parameters for this test case remain the same as in Test Case 1. However, in this case, two uncertainties exist at the boundary heads, and two pressure sensors are placed at nodes 1 and 3. This scenario is more realistic and can happen in pipeline networks, where head measurements may be available at some locations, but the heads at other boundaries remain unknown and require estimation.

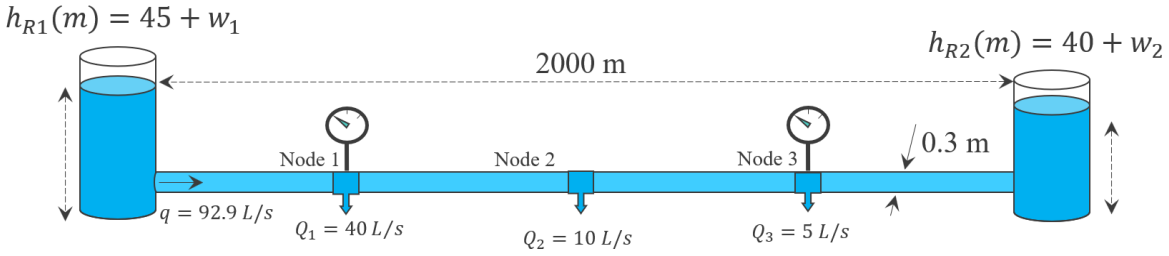

Fig. 7. Pipeline configuration for Test Case 2. The wave speed is 1000 m/s and friction factor is 0.02.

For the state-space model, the $\boldsymbol{A}$ and $\boldsymbol{B}$ matrices remain unchanged from Test Case 1, while the $\boldsymbol{D}$ and $\boldsymbol{C}$ has been obtained as below:

$$\boldsymbol{D} = \begin{bmatrix} 0.0014 & 0 \\ 0 & 0 \\ 0 & 0 \\ 0 & -0.0014 \\ 0 & 0 \\ 0 & 0 \\ 0 & 0 \end{bmatrix} \quad \boldsymbol{C} = \begin{bmatrix} \boldsymbol{C}_1 \\ \boldsymbol{C}_2 \end{bmatrix} = \begin{bmatrix} 0 & 0 & 0 & 0 & 1 & 0 & 0 \\ 0 & 0 & 0 & 0 & 0 & 0 & 1 \end{bmatrix}$$

The rank of the $\boldsymbol{CD}$ matrix is zero, confirming that auxiliary outputs are required. Using Eq. (15), the relative degree for each output is computed as 1, meaning only one auxiliary output per sensor is required. The augmented output is obtained in the following format:

$$\boldsymbol{y}_a = \boldsymbol{C}_a \boldsymbol{x} = \begin{bmatrix} \boldsymbol{C}_1 \\ \boldsymbol{C}_1\boldsymbol{A} \\ \boldsymbol{C}_2 \\ \boldsymbol{C}_2\boldsymbol{A} \end{bmatrix} \boldsymbol{x}$$

Two HGOs are designed with parameters $\varepsilon = 0.001$ and $\alpha_{a,1:2} = [1,3]$ to estimate the auxiliary outputs. Two uncertainties are introduced at both boundary heads, simulating real-world conditions where boundary conditions are not precisely known.

After applying the method, Fig. 8 shows the estimation errors for the auxiliary outputs $y_{a1,2}$ and $y_{a2,2}$ which correspond to the first derivatives of the first and second measured output signals, respectively. The errors are on the order of 10^{-3}. The error can be further reduced by decreasing ε.

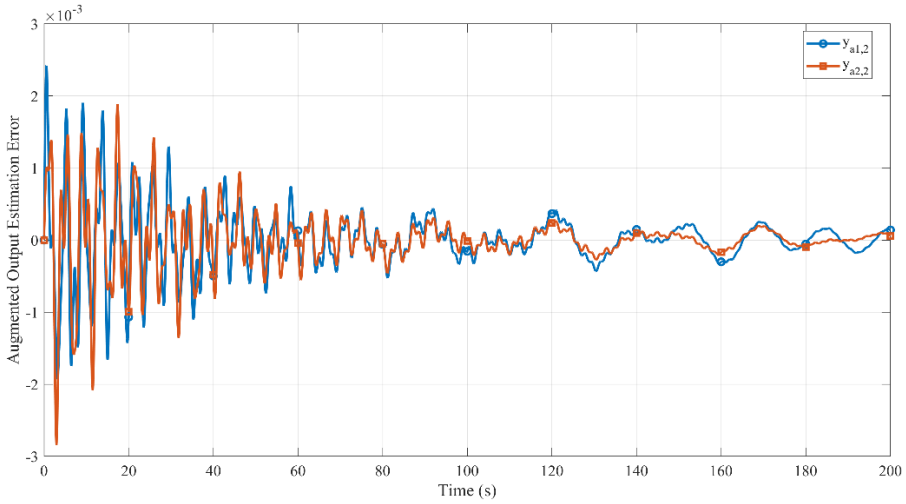

Fig. 8. Auxiliary output estimation error.

The estimated auxiliary outputs are then fed into the SMO, which provides the disturbance and state estimations, as shown in Fig. 9 and Fig. 10. Both disturbances are estimated with high accuracy, closely tracking the actual disturbances. Alongside disturbance estimation, the system states are also successfully reconstructed. As shown in Fig. 10, the estimated pressure at internal nodes closely matches the results from the true simulation.

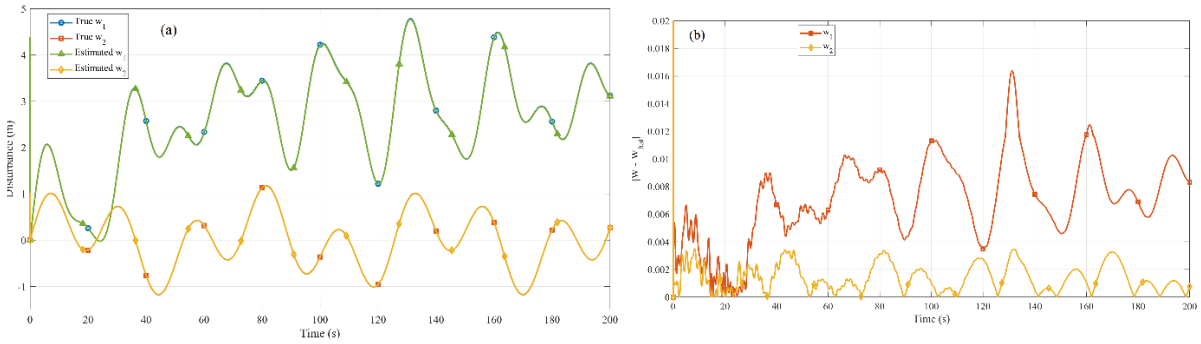

Fig. 9. Disturbance estimation results for Test Case 1: (a) comparison of true and estimated disturbances, and (b) absolute estimation errors.

388

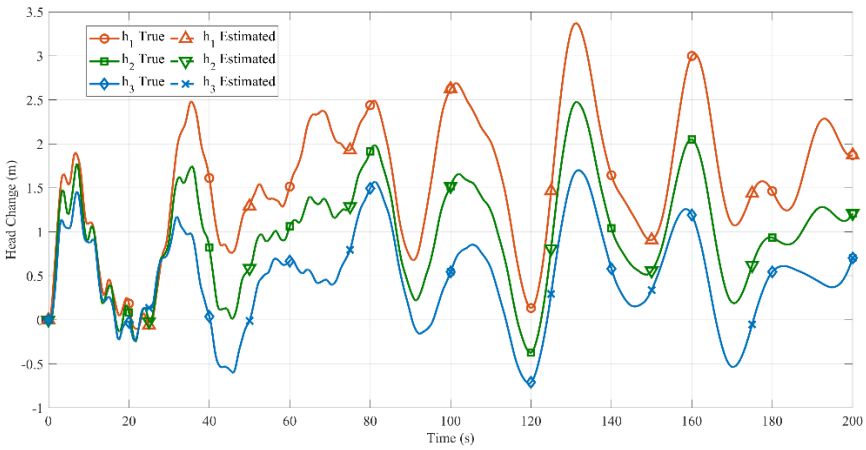

Fig. 10. True and estimated internal pressure head state variables for Test Case 2.

389 ## Experimental Verification

390 A laboratory experiment was conducted to demonstrate the practical performance of the
391 proposed estimation method. The setup is located in the Robin Hydraulics Laboratory at the
392 University of Adelaide. The layout of the experimental system is shown in Fig. 11, consisting
393 of two tanks positioned at either end of a copper pipeline. The system includes two internal
394 measurement points along the pipeline and two additional measurement points near the
395 boundary tanks, which closely represent the head at the tank boundaries.

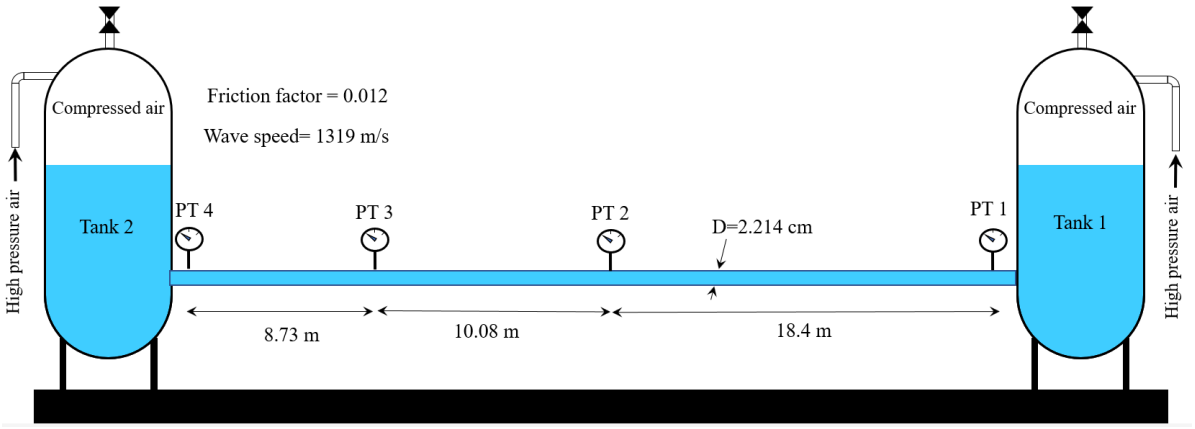

Fig. 11. Experimantal pipeline setup.

In this experiment, both tanks were initially pressurized to 10 meters of head, and the pressure was held constant for a sufficient duration to ensure steady-state conditions. Under this operating point, the flow in the pipe is effectively zero, and all four pressure transducers report the same value. To induce a transient event, the pressure at Tank 1 was varied arbitrarily. As a result, the generated flow caused the pressure at Tank 2 to gradually change over time. These boundary pressures can be considered as unknown inputs.

The objective of the experiment was to use the pressure readings from the two internal measurement points along the pipeline to estimate the unknown boundary conditions, following the same estimation strategy applied in Test Case 2 using a SMO. The SMO was designed to reconstruct the head at both boundaries in real time.

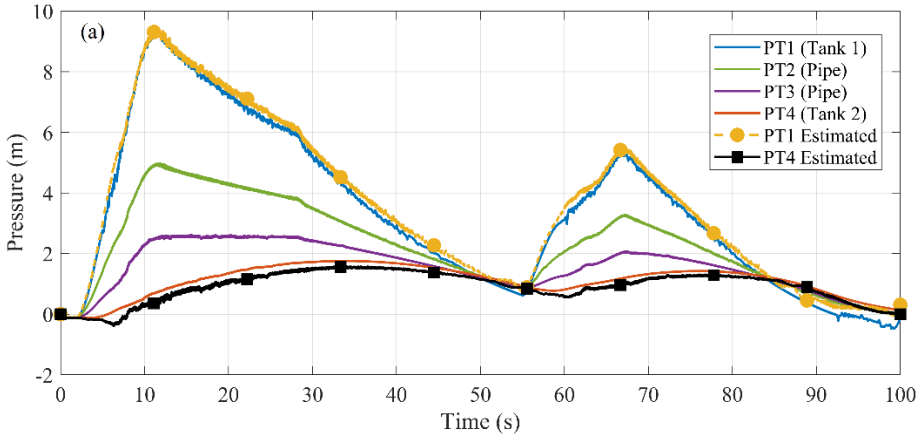

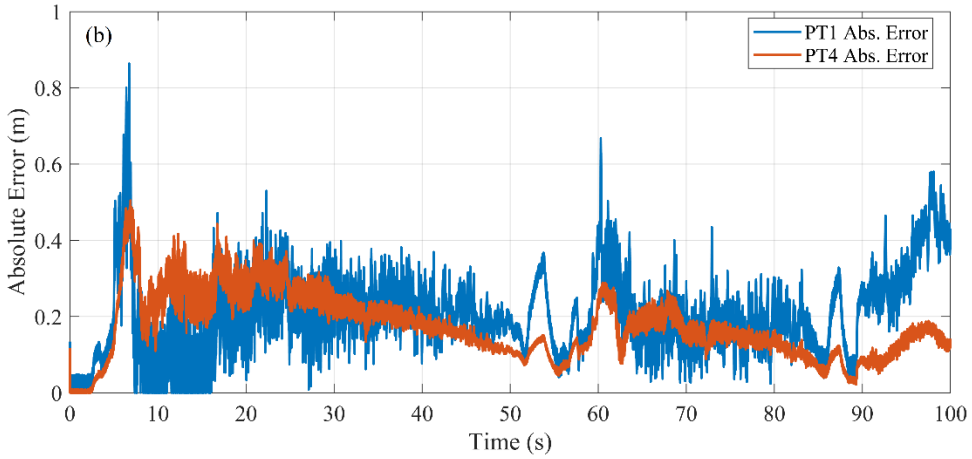

Fig. 12. Experimental results of boundary pressure estimation. (a) Measured and estimated pressures at PT1 and PT4 (tanks), with PT2 and PT3 shown for reference. (b) Absolute estimation errors for PT1 and PT4.

Fig. 12(a) presents the comparison between the measured and estimated boundary pressures. It is important to note that in any experimental validation, discrepancies can exist between the mathematical model and the physical system. In this case, the EWCM is used as an approximate representation of the real pipeline behavior. Therefore, part of the observed error may be due to modeling limitations rather than the estimation process itself. Despite this, the observer was able to track arbitrary changes at the boundaries with an error of less than 10%, demonstrating good estimation performance. The corresponding absolute estimation error is also shown in Fig. 12b. Several sources of uncertainty contribute to this error. First, there is inherent uncertainty in parameters such as wave speed and friction factor. Second, the estimation is based on a linearized approximation of the system, while the real dynamics remain nonlinear. Third, measurement noise can affect the accuracy of auxiliary output estimation. Overall, the results confirm that the proposed estimation method remains effective under realistic model uncertainty and sensor conditions.

Fig. 13 shows the estimated flow rate at one section of the pipe over time. As the pipe is relatively short and has no discharge along its length, the flow rate is uniform across all sections at any given time; therefore, a single representative section is shown. This estimation approach

uses only pressure readings to infer the flow rate, eliminating the need for direct flow measurements, which are typically more expensive and difficult to implement in practice.

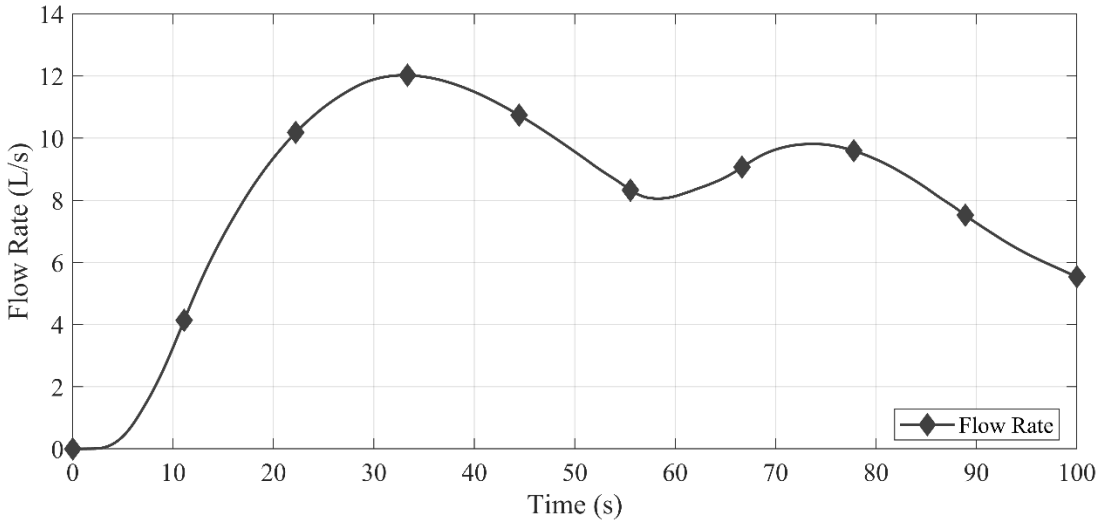

Fig. 13. Estimated flow rate over time for the experimental pipeline.

Conclusion

This paper presents a state estimation and uncertainty reconstruction framework for pressurized pipeline systems. The proposed method addresses the limitation imposed by the observer matching condition by introducing auxiliary outputs generated via a HGO. These outputs are then used within a SMO to reconstruct both system states and unknown boundary conditions in real time. The framework has been evaluated through numerical simulations and experimentally validated using laboratory data, demonstrating its ability to estimate slowly varying transients with reasonable accuracy despite model uncertainties and measurement noise.

This approach offers a practical solution for real-time monitoring and control in systems where boundary conditions are not fully observed. In particular, it holds promise for application in water distribution networks, where multiple sources of uncertainty, such as unmeasured demands, pressure fluctuations, and operational changes, are common. By enabling real-time estimation without relying on optimization routines or statistical noise models, the proposed method provides a computationally efficient alternative to traditional techniques.

To extend this approach to pipeline networks, further development is required. As networks introduce greater complexity and interconnectivity, the number of necessary auxiliary outputs is expected to increase, potentially requiring more advanced observer structures. Based on the framework developed in this study, future research can also explore distributed observer designs that are better suited to large-scale water distribution networks with decentralized sensing and control. Future work will focus on scaling the method to larger networks, assessing robustness to parameter uncertainties, and integrating the observer into active control schemes for fault detection and operational optimization.

Acknowledgements

This research is funded by the Australian Research Council through the Discovery Project Grant DP230101513.

Data Availability Statement

Some or all data, models, or code that support the findings of this study are available from the corresponding author upon reasonable request.

References

[1] G. Palli, S. Strano, M. Terzo, A novel adaptive-gain technique for high-order sliding-mode observers with application to electro-hydraulic systems, Mechanical Systems and Signal Processing, 144 (2020) 106875.
[2] H. Cheng, X. Li, J. Jiang, Z. Deng, J. Yang, J. Li, A nonlinear sliding mode observer for the estimation of temperature distribution in a planar solid oxide fuel cell, International Journal of Hydrogen Energy, 40 (2015) 593-606.
[3] B. Wang, X. Yu, L. Mu, Y. Zhang, Disturbance observer-based adaptive fault-tolerant control for a quadrotor helicopter subject to parametric uncertainties and external disturbances, Mechanical Systems and Signal Processing, 120 (2019) 727-743.
[4] P.J. Lee, J.P. Vítkovský, M.F. Lambert, A.R. Simpson, J.A. Liggett, Leak location using the pattern of the frequency response diagram in pipelines: a numerical study, Journal of Sound and Vibration, 284 (2005) 1051-1073.

[5] P.J. Lee, J.P. Vítkovský, M.F. Lambert, A.R. Simpson, J.A. Liggett, Leak location in pipelines using the impulse response function, Journal of Hydraulic Research, 45 (2007) 643-652.
[6] A.C. Zecchin, M.F. Lambert, A.R. Simpson, L.B. White, Parameter Identification in Pipeline Networks: Transient-Based Expectation-Maximization Approach for Systems Containing Unknown Boundary Conditions, Journal of Hydraulic Engineering, 140 (2014) 04014020.
[7] C. Zhang, M.F. Lambert, J. Gong, A.C. Zecchin, A.R. Simpson, M.L. Stephens, Bayesian Inverse Transient Analysis for Pipeline Condition Assessment: Parameter Estimation and Uncertainty Quantification, Water Resources Management, 34 (2020) 2807-2820.
[8] A.C. Zecchin, L.B. White, M.F. Lambert, A.R. Simpson, Parameter identification of fluid line networks by frequency-domain maximum likelihood estimation, Mechanical Systems and Signal Processing, 37 (2013) 370-387.
[9] H. Kim Sang, Address-Oriented Impedance Matrix Method for Generic Calibration of Heterogeneous Pipe Network Systems, Journal of Hydraulic Engineering, 134 (2008) 66-75.
[10] C. Capponi, M. Ferrante, A.C. Zecchin, J. Gong, Leak Detection in a Branched System by Inverse Transient Analysis with the Admittance Matrix Method, Water Resources Management, 31 (2017) 4075-4089.
[11] D. Luenberger, Observers for multivariable systems, IEEE Transactions on Automatic Control, 11 (1966) 190-197.
[12] S. Venkateswaran, C. Kravaris, Linear Unknown Input Observers for Sensor Fault Estimation in Nonlinear Systems, IFAC-PapersOnLine, 56 (2023) 61-66.
[13] G. Yang, A. Barboni, H. Rezaee, T. Parisini, State estimation using a network of distributed observers with unknown inputs, Automatica, 146 (2022) 110631.
[14] M. Hou, P.C. Muller, Design of observers for linear systems with unknown inputs, IEEE Transactions on Automatic Control, 37 (1992) 871-875.
[15] A. Mitra, S. Sundaram, Distributed Observers for LTI Systems, IEEE Transactions on Automatic Control, 63 (2018) 3689-3704.
[16] F. Zhu, M. Li, Distributed Interval Observer and Distributed Unknown Input Observer Designs, IEEE Transactions on Automatic Control, 69 (2024) 8868-8875.
[17] J. Zhang, Y. Song, G. Zheng, Prescribed-time observer for descriptor systems with unknown input, Automatica, 172 (2025) 111999.
[18] J. Zhang, X. Zhao, G. Zheng, F. Zhu, T.N. Dinh, On Distributed Prescribed-Time Unknown Input Observers, IEEE Transactions on Automatic Control, 70 (2025) 4743-4750.
[19] S.K.S. Christopher Edwards, Sliding Mode Control: Theory And Applications, CRC Press, 1998.
[20] C. Edwards, S.K. Spurgeon, C.P. Tan, On the Development and Application of Sliding Mode Observers, in: X. Yu, J.-X. Xu (Eds.) Variable Structure Systems: Towards the 21st Century, Springer Berlin Heidelberg, Berlin, Heidelberg, 2002, pp. 253-282.
[21] T. Floquet, J.-P. Barbot, State and unknown input estimation for linear discrete-time systems, Automatica, 42 (2006) 1883-1889.
[22] T. Floquet, C. Edwards, S.K. Spurgeon, On Sliding Mode Observers for Systems with Unknown Inputs, International Workshop on Variable Structure Systems, 2006. VSS'06., 2006, pp. 214-219.
[23] K. Kalsi, J. Lian, S. Hui, S.H. Żak, Sliding-mode observers for systems with unknown inputs: A high-gain approach, Automatica, 46 (2010) 347-353.
[24] X. Wang, C.P. Tan, Output Feedback Active Fault Tolerant Control for a 3-DOF Laboratory Helicopter With Sensor Fault, IEEE Transactions on Automation Science and Engineering, 21 (2024) 2689-2700.
[25] X. Wang, C.P. Tan, D. Zhou, A novel sliding mode observer for state and fault estimation in systems not satisfying matching and minimum phase conditions, Automatica, 79 (2017) 290-295.
[26] X. Wang, C.P. Tan, Y. Wang, Q. Qi, X. Wang, Adaptive Interval Observer-Based Fault-Tolerant Control for a 3-DOF Helicopter Without Angular Velocity Measurement, IEEE Transactions on Control Systems Technology, (2025) 1-7.
[27] F. Zhu, Y. Fu, T.N. Dinh, Asymptotic convergence unknown input observer design via interval observer, Automatica, 147 (2023) 110744.
[28] J. Zhang, F. Zhu, On the observer matching condition and unknown input observer design based on the system left-invertibility concept, Transactions of the Institute of Measurement and Control, 40 (2017) 2887-2900.
[29] E.B. Wylie, and V. L. Streeter, Fluid transients in systems, Prentice Hall., Englewood Cliffs, 1993.
[30] O.H. Souza, N. Barbieri, A.H.M. Santos, Study of hydraulic transients in hydropower plants through simulation of nonlinear model of penstock and hydraulic turbine model, IEEE Transactions on Power Systems, 14 (1999) 1269-1272.
[31] W. Zeng, C. Zecchin Aaron, F. Lambert Martin, Elastic Water Column Model for Hydraulic Transient Analysis of Pipe Networks, Journal of Hydraulic Engineering, 148 (2022) 04022027.
[32] C. Nicolet, Hydroacoustic modelling and numerical simulation of unsteady operation of hydroelectric systems, Dept. Mechanical Engineering, Ph.D. thesis, Swiss Federal Institute of Technology Lausanne, 2007.

[33] G. Franklin, J. Powell, A. Emami-Naeini, Feedback Control of Dynamic Systems, Prentice-Hall, 2010.
[34] C. Edwards, S.K. Spurgeon, R.J. Patton, Sliding mode observers for fault detection and isolation, Automatica, 36 (2000) 541-553.
[35] F. Esfandiari, H.K. Khalil, Output feedback stabilization of fully linearizable systems, International Journal of Control, 56 (1992) 1007-1037.
[36] N.A. Mahmoud, H.K. Khalil, Asymptotic regulation of minimum phase nonlinear systems using output feedback, IEEE Transactions on Automatic Control, 41 (1996) 1402-1412.
[37] S.K. Spurgeon, Sliding mode observers: a survey, International Journal of Systems Science, 39 (2008) 751-764.